

# Bayesian Critique-Tune-Based Reinforcement Learning with Attention-Based Adaptive Pressure for Multi-Intersection Traffic Signal Control

Wenchang Duan, Zhenguo Gao, Jinguo Xian

**Abstract**—Adaptive Traffic Signal Control (ATSC) system is a critical component of intelligent transportation, with the capability to significantly alleviate urban traffic congestion. Although reinforcement learning (RL)-based methods have demonstrated promising performance in achieving ATSC, existing methods find it prone to convergence to local optima. Consequently, this paper proposes a novel Bayesian Critique-Tune-Based Reinforcement Learning with Attention-Based Adaptive Pressure (BCT-APRL) for multi-intersection signal control. In BCT-APRL, the Critique-Tune (CT) framework, a two-layer Bayesian structure is designed to refine the RL policies. Specifically, the Bayesian inference-based Critique layer provides effective evaluations of the credibility of policies; the Bayesian decision-based Tune layer fine-tunes policies by minimizing the posterior risks when the evaluations are negative. Furthermore, an attention-based Adaptive Pressure (AP) is designed to specify the traffic movement representation as an effective and efficient pressure of vehicle queues in the traffic network. Achieving enhances the reasonableness of RL policies. Extensive experiments conducted with a simulator across a range of intersection layouts show that BCT-APRL is superior to other state-of-the-art methods in seven real-world datasets. Codes are open-sourced.

**Index Terms**—Traffic signal control, Reinforcement learning, Bayesian Critique-Tune, Adaptive pressure.

## I. INTRODUCTION

WITH urban populations continuous growth and cities expanding, traffic congestion has become increasingly severe, placing escalating pressure on the environment and economy [1]–[3]. As a significant component of transportation systems, ATSC system can effectively alleviate traffic congestion via real-time dynamic control of signals [4]–[6]. Reinforcement learning (RL) has been extensively explored as an efficient method in the ATSC system [7] [8]. However, the increasingly complex traffic demands of modern cities have outpaced the capabilities of existing RL-based methods [9]–[11]. Most methods struggle to formulate optimal policies when confronted with complex traffic environments [12]–[15]. Therefore, it is crucial to accurately capture the traffic states and make sure the RL policies achieve global optima.

By effectively optimizing long-term returns and enabling dynamic interactions with environments, RL has demonstrated promising performance [16]–[18]. Specifically, references [19]

[20] employed the independently RL agent at each intersection to improve the scalability issues. References [21] [22] introduced graph networks into RL, which implemented parameter sharing mechanisms to incorporate temporal and spatial influences from neighboring intersections. Da et al. [23] proposed the PromptGAT method to bridge the simulation-to-reality performance gap. However, the above methods placed excessive trust in RL policies, which often theoretically fail to convergence [24]. Furthermore, the lack of effective traffic states representation causes existing methods huge difficulties for the rationality of RL policies.

To address the unreasonableness of the RL policies, much literature has focused on how to enhance the reliability of the learning process [25]. Specifically, Wang et al. proposed a cooperative double Deep Q-Network (DQN) method [26] to improve the robustness of the learning process. Hinton et al. proposed a teacher-student framework [27], in which the teacher module guides the student module to avoid major errors in the learning process. And references [28], [29] addressed the limitation of traditional teacher-student advising methods, which only offered advice in situating the same state or after having similar experiences. Furthermore, references [30]–[32] introduced the A2C algorithm, allowing for the evaluation and adjustment of the learning process. References [33], [34] proposed the multi-objective Bayesian optimization to solve the model-free problem in the learning process. However, the aforementioned methods simply focus on the learning process while overlooking the policy-making process, which often leads to unreasonable or suboptimal RL policies.

In the ATSC system, effective and efficient traffic states representation is also the key, rather than only complex algorithms [7] [8]. To efficiently represent the traffic scenario, references [35]–[37] developed methods to quantify complex traffic information based on the max-pressure theory. Wu et al. [38] introduced the concept of efficient pressure to represent traffic states, achieving notable efficiency in signal control. Zhang et al. [39] further incorporated both waiting and running vehicles to enhance the comprehensiveness of traffic states representation. However, the existing pressure calculation methods overlook the varying influence of multiple upstream lanes on each downstream lane. This limitation may amplify the impact of low-traffic lanes while reducing responsiveness to high-traffic ones. Although computationally efficient, existing methods lack adaptability to dynamic traffic, undermining the rationality of RL policies.

According to the above analysis, the excessive trust of RL

Wenchang Duan, Zhenguo Gao and Jinguo Xian are with the School of Mathematical Sciences, Shanghai Jiao Tong University, China (duanwengang@sjtu.edu.cn, gaozheng@sjtu.edu.cn, jgxian@sjtu.edu.cn). Correspondence to: Zhenguo Gao. This work is supported by National Natural Science Foundation of China (Grant No. NSFC-12001365).

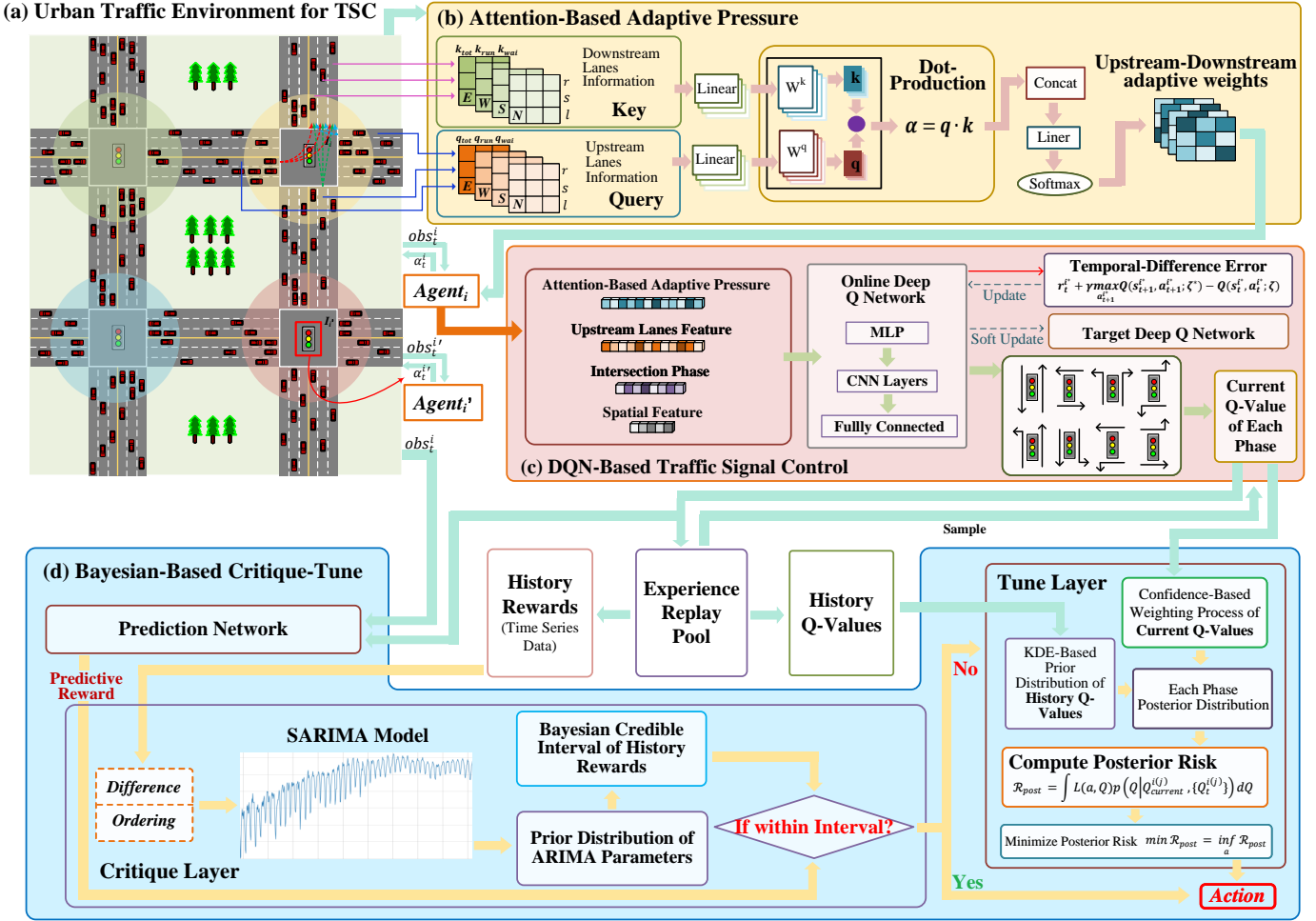


Fig. 1: Architecture of BCT-APRL. The urban traffic environment for ATSC (a) offers complex traffic dynamics and an interactive framework for reinforcement learning (RL). Attention-based Adaptive Pressure (b) enables RL agents to effectively capture traffic states. This adaptive pressure, combined with traffic lane details, enhances DQN-based traffic signal control (c). The Bayesian-based Critique-Tune framework (d) evaluates and refines RL policies for improved decision-making.

policies and the ineffectiveness of traffic states representation severely limit the formulation of reasonable policies. To address these problems, this paper proposes a Bayesian Critique-Tune-Based Reinforcement Learning with Attention-Based Adaptive Pressure (BCT-APRL) for multi-intersection signal control. The framework of the BCT-APRL is shown in Fig. 1. Firstly, the Critique-Tune (CT) framework employs a two-layer Bayesian structure to refine RL policies. Specifically, the Bayesian inference-based Critique layer constructs a Bayesian credible interval, which uses historical rewards to evaluate current policies. If the evaluation is negative, the Bayesian decision-based Tune layer calculates the posterior risk of each phase according to the posterior probability of Q-values. By minimizing this risk, the Tune layer fine-tunes the policies. In addition, the Attention-based Adaptive Pressure is designed for computing pressure and representing the states of complex traffic, which achieves being effective in ATSC. With the above designs, the BCT-APRL can effectively adjust the pending policies and handle the complex traffic states.

The contributions of this paper can be summarized as follows.

- This paper proposes a Bayesian Critique-Tune-based Attention Reinforcement Learning for traffic signal control. Equipped with a Critique-Tune framework, BCT-APRL achieves refinement of the pending RL policies, encouraging convergence to the global optima.
- An Attention-based Adaptive Pressure is proposed to effectively capture the traffic states, achieving effective and efficient traffic states representation in real time, thereby helping policy-making rationally.
- This paper conducts extensive experiments on real-world traffic datasets and compares BCT-APRL with existing traditional, RL-based and LLM-based ATSC methods. The experimental results demonstrate that BCT-APRL provides an effective and efficient traffic signal control strategy.

## II. TRAFFIC SIGNAL CONTROL WITH REINFORCEMENT LEARNING IN URBAN INTERSECTIONS

This section describes the concepts and methodology relevant to this paper. Firstly, key definitions related to ATSC are provided in Subsection II-A. Following that, Subsection

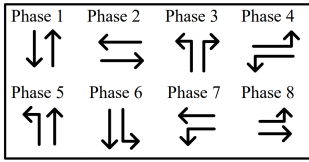
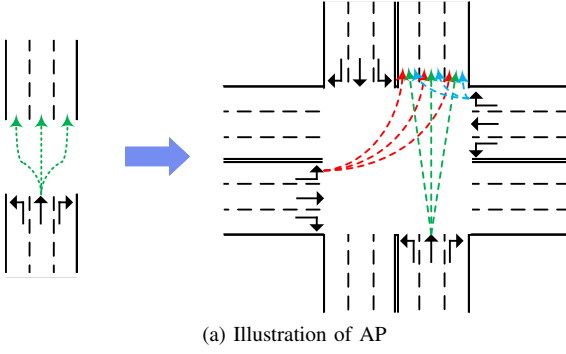


Fig. 2: The traditional efficient pressure and the attention-based adaptive pressure are provided in (a). The eight traffic signals are illustrated in (b).

II-B introduces the mathematical framework of reinforcement learning for ATSC. Based on these concepts and methodology, this paper researches adaptive traffic signal control across multi-intersections to minimize average travel time.

#### A. ATSC Definition in Multi-Intersections

**Definition 1 (Traffic Intersection and Road):** The traffic network can be modeled as a directed graph, where nodes correspond to  $n$  number of intersections  $I$  and edges represent roads. At each intersection  $I_i$ , the road network consists of four directions  $\{E, W, S, N\}$ : east ( $E$ ), west ( $W$ ), south ( $S$ ), and north ( $N$ ).

**Definition 2 (Traffic Lanes):** Traffic road networks typically comprise three distinct types of lanes: left-turn *lef*, straight-through *str*, and right-turn *rig*. The traffic lanes in an intersection  $I_i$  can be described as the upstream lanes  $\{X_{y'}^i\}$  and downstream lanes  $\{X_y^i\}$ , in which  $X, X' \in \{E, W, S, N\}$  and  $y, y' \in \{lef, str, rig\}$ . Specifically, the vehicles enter the intersection  $I_i$  are denoted as the upstream lanes  $\{X_{y'}^i\}$ , and the vehicles leave the intersection  $I_i$  are denoted as the downstream lanes  $\{X_y^i\}$ .

**Definition 3 (Traffic Movement):** Traffic movement is defined as the flow of traffic crossing an intersection from one upstream lane to one downstream lane. A traffic movement, such as from lane  $X_y^i$  to lane  $X_{y'}^i$ , is denoted as  $(X_y^i, X_{y'}^i)$ . At an intersection where each road comprises three lanes, one downstream lane has three upstream lanes to generate traffic movements, thereby a total of nine traffic movements for one road that includes three downstream lanes.

**Definition 4 (Traffic Queue Length):** The traffic queue length  $x(X_y^i)$  represents the number of vehicles waiting in lane  $X_y^i$ .

**Definition 5 (Traffic running vehicle number):** The traffic running vehicle number  $r(X_y^i)$  represents the number of vehicles running in lane  $X_y^i$ .

**Definition 6 (Traffic Signal Phase):** Each traffic signal phase represents a set of allowed traffic movements. The sum of phases in intersection  $I_i$  is denoted as  $J_i$ , and notation  $j$  is used to denote one of the phases. Fig. 2(b) demonstrates the mostly used eight phases.

**Definition 7 (Efficient pressure):** The efficient pressure (EP) is the difference between the average queue length on upstream lanes and the average queue length on downstream lanes.

$$p_e(X_y^i, X_{y'}^i) = \frac{1}{L} \sum_{l_k} x(l_k) - \frac{1}{M} \sum_{m_j} x(m_j) \quad (1)$$

where  $l_k \in \{X_y^i\}$ ,  $m_j \in \{X_{y'}^i\}$ ,  $L$  and  $M$  represent the number of lanes of  $\{X_y^i\}$  and  $\{X_{y'}^i\}$ . The schema is shown in the left part of Fig. 2(a).

**Definition 8 (Adaptive pressure):** The attention-based adaptive pressure (AP) is the difference between the queue length at each upstream lane and the weighted queue length on downstream lanes.

$$p_e(X_y^i, X_{y'}^i) = x(l_k) - \sum_{j=1}^M \omega_j^k x(m_j) \quad (2)$$

where  $l_k \in \{X_y^i\}$ ,  $m_j \in \{X_{y'}^i\}$ ,  $M$  represents the number of lanes of  $\{X_{y'}^i\}$ , and  $\omega_j^k$  represents the weight of vehicle flow of upstream lane  $l_k$  on downstream lane  $m_j$ . The schema is shown in the right part of Fig. 2(a).

#### B. Markov property in RL-based ATSC

Due to their shared Markov property, RL is commonly modeled using the Markov process. Wherein state transitions depend solely on the current state but are independent of historical states. This characteristic enables RL to be effectively formulated as a Markov Decision Process (MDP), facilitating the optimization of policies to maximize the expected cumulative reward. Therefore, at time  $t$  in intersection  $I_i$ , RL is composed of six fundamental elements: the state space  $\mathcal{S} = \{s_t^1, \dots, s_t^n\}$ , observation space  $\mathcal{O} = \{o_t^1, \dots, o_t^n\}$ , action space  $\mathcal{A} = \{a_t^1, \dots, a_t^n\}$ , transition probability function  $P(s_t^{i'} | s_t^i, a_t^i)$ , reward function  $R(s_t^i, a_t^i) = \{r_t^1, \dots, r_t^n\}$ , and discount factor  $\gamma$ .

The goal of MDP is to make global optima policies  $\pi = \{\pi_t^1, \dots, \pi_t^n\}$ , under each intersection  $I_i$  to maximize the own expected cumulative reward of taking a specific action  $a_t^i$  in a given state  $s_t^i$  over all future time steps, i.e., the state value function:

$$V(s_t^i) = \mathbb{E}_{\pi_t^i} \left[ \sum_{k=0}^{\infty} \gamma^k r_{t+k+1}^i | s_t^i \right] \quad (3)$$

where  $\pi_t^i: o_t^i \times a_t^i \rightarrow [0, 1]$  maps the observation of intersection  $I_i$  to the probability distribution of its action. The Q-value (action-value) of each intersection is defined as

$$Q(s_t^i, a_t^i) = \mathbb{E}_{\pi_t^i} \left[ \sum_{k=0}^{\infty} \gamma^k r_{t+k+1}^i | s_t^i, a_t^i \right] \quad (4)$$

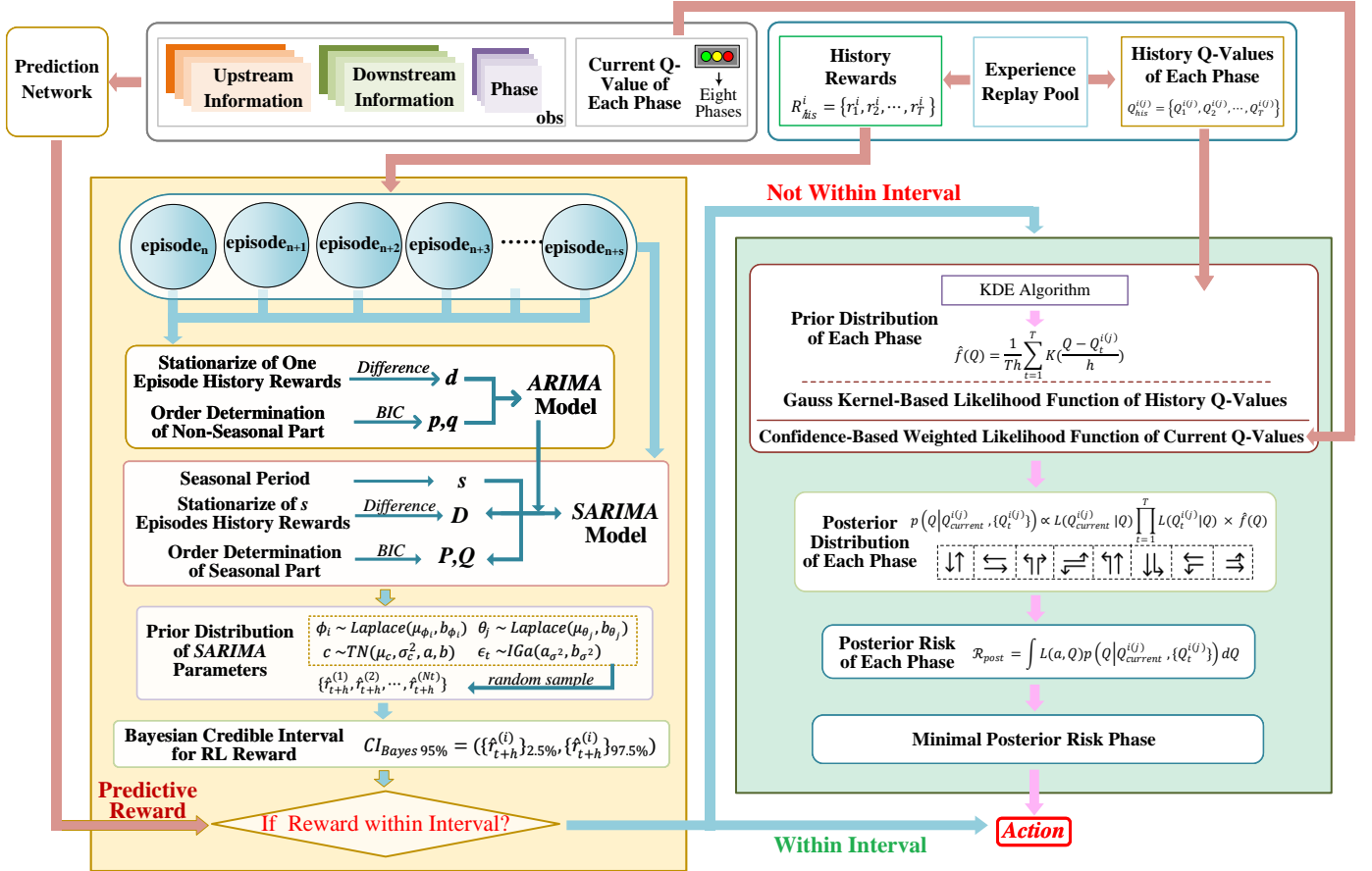


Fig. 3: Architecture of Bayesian Critique-Tune for RL.

Q-learning is a classic RL algorithm that aims to find the optimal action-selection policy by iteratively updating Q-values based on the Bellman equation [40]. The update rule is expressed as

$$Q(s_t^i, a_t^i) \leftarrow Q(s_t^i, a_t^i) + \alpha \eta_t^i \quad (5)$$

where  $\alpha$  is the learning rate and

$$\eta_t^i = \left[ r_t^i + \gamma \max_{a_{t+1}^i} Q(s_{t+1}^i, a_{t+1}^i) - Q(s_t^i, a_t^i) \right] \quad (6)$$

For each intersection  $I_i$ , the RL agent calculates the expected Q-values for eight phases. This process derives optimal policies to enhance traffic efficiency.

### III. BAYESIAN CRITIQUE-TUNE FRAMEWORK FOR RL

To achieve the RL policies of convergence to the global optima, this paper designs a two-layer Bayesian structure to refine RL policies. Subsection III-A describes the overall structure. Subsection III-B provides an in-depth discussion of the Critique Layer and Subsection III-C presents the Tune Layer in detail.

#### A. Bayesian Critique-Tune Structure

The policy-making process is vital for achieving global optima, enabling RL agents to deal with the complex urban traffic

effectively. Consequently, this paper proposes the Critique-Tune (CT) framework, a two-layer Bayesian structure to refine the RL policies, as shown in Fig. 3.

In this framework, an auxiliary prediction network is implemented to predict the predictive reward  $r_{t+h}^i$  corresponding to the next action. Equipped with the current Q-value  $Q_{cur}^i$  and environment observation shared from the DQN, the prediction network is capable of generating the most suitable predictive reward, aligning its generation logic consistently with the DQN.

Concurrently, the Bayesian inference-based Critique layer constructs a credible interval  $CI_{Bayes}$  by utilizing historical rewards  $R_{his}^i = \{r_1^i, r_2^i, \dots, r_T^i\}$  and Bayesian prior experience. This interval evaluates whether the predictive reward  $r_{t+h}^i$  falls within an acceptable range based on prior knowledge. Subsequently, the Bayesian decision-based Tune layer is activated if the evaluation yields a negative outcome, which meaning that  $r_{t+h}^i \notin CI_{Bayes}$ . For each phase, the Tune layer computes the posterior risk  $\mathcal{R}_{post}$  by integrating the posterior distribution  $p(Q | Q_{his}^{(j)}, Q_{cur}^{(j)})$  of the history Q-values  $Q_{his}^{(j)} = \{Q_1^{(j)}, Q_2^{(j)}, \dots, Q_T^{(j)}\}$  and current Q-value  $Q_{cur}^{(j)}$ , in which  $j = 1, 2, \dots, 8$  denoted as each phase. Via selecting the phase with the minimal posterior risk  $\min \mathcal{R}_{post}$ , the Tune layer ensures the updated policy  $\pi_{upd}^i$  is more aligned with the global optima.

## B. The Critique Layer

The Bayesian inference-based Critique Layer is responsible for evaluating the reasonableness of RL policies. Its judging process is divided into three main sections.

1) *SARIMA Modeling of History Rewards*: In this section, the history rewards  $R_{his}^i$  of RL are subjected to rigorous time series analysis. Thus, it can be mathematically represented using a time series model. Initially, the Augmented Dickey-Fuller (ADF) test is employed to judge the stationarity of the history rewards data. If the data exhibits non-stationarity, an appropriate *differencing* process is applied. Typically, the expression for a  $d$ -th order *differencing* is given by:

$$w_t^{i(d)} = (1 - B)^d r_t^i \quad (7)$$

where  $r_t^i$  and  $w_t^{i(d)}$  represent the original and *differenced* history rewards data,  $B$  is the lag operator that defined as  $Br_t^i = r_{t-1}^i$ , and  $d$  denotes the *differencing* order.

When the history reward data is transformed into a stationary time series, the long-term dependence properties within a single episode of RL-based ATSC can be modeled using an Autoregressive Integrated Moving Average (ARIMA) model. Each episode's data can then be represented by the ARIMA equation:

$$\left(1 - \sum_{k=1}^p \phi_k B^k\right) (1 - B)^d r_t^i = \left(1 + \sum_{j=1}^q \theta_j B^j\right) \epsilon_t \quad (8)$$

where  $\phi_i$  represents the autoregressive coefficients,  $\theta_j$  represents the moving average coefficients,  $\epsilon_t$  represents the random error term at time  $t$  and typically assumed to be white noise (i.e.  $\epsilon_t \sim \mathcal{N}(0, \sigma^2)$ ). Moreover,  $p$  denotes the order of the autoregressive (AR) part, and  $q$  denotes the order of the moving average (MA) part.

Subsequently, the optimal orders  $\{p, d, q\}$  of the ARIMA model need to be determined, tailored to the complexities inherent in RL-based ATSC. The determination process uses the Bayesian Information Criterion (BIC) to evaluate and select the model order, balancing complexity and predictive accuracy. The BIC formulation is given as follows:

$$\text{BIC} = -2 \ln(L) + k \ln(n) \quad (9)$$

where  $L$  is the likelihood function value of the model, and  $k$  represents the number of parameters in the ARIMA model.

In order to enhance the rationality of the credible interval, this paper introduces the Seasonal Autoregressive Integrated Moving Average (SARIMA) model to fit the multi-episodes data, with each episode regarded as the same ARIMA model (the detailed proof is presented in Appendix A). In detail, the SARIMA model combines non-seasonal and seasonal components, which are the non-seasonal part ARIMA( $p, d, q$ ) and the seasonal part SARIMA( $P, D, Q, s$ ). The non-seasonal part of ARIMA ( $p, d, q$ ) is defined as above. The definitions of the seasonal part of SARIMA( $P, D, Q, s$ ) are as follows:  $P$  denotes the order of the seasonal autoregressive part,  $Q$  denotes the order of the seasonal moving average part,  $D$  denotes the seasonal *differencing* order, and  $s$  denotes the seasonal period. The optimal orders  $\{P, D, Q\}$  also determined by Eq. (9).

Building on the above methods, the SARIMA equation for historical rewards in the traffic signal control context can be modeled:

$$\Phi_P(B^s) \phi_p(B) \nabla^d \nabla_s^D r_t^i = \Theta_Q(B^s) \theta_q(B) \epsilon_t \quad (10)$$

where  $\phi_p(B) = 1 - \phi_1 B - \phi_2 B^2 - \dots - \phi_p B^p$ ,  $\Phi_P(B^s) = 1 - \Phi_1 B^s - \Phi_2 B^{2s} - \dots - \Phi_P B^{Ps}$ ,  $\nabla^d r_t^i = (1 - B)^d r_t^i$ ,  $\nabla_s^D r_t^i = (1 - B^s)^D r_t^i$ ,  $\theta_q(B) = 1 + \theta_1 B + \theta_2 B^2 + \dots + \theta_q B^q$ ,  $\Theta_Q(B^s) = 1 + \Theta_1 B^s + \Theta_2 B^{2s} + \dots + \Theta_Q B^{Qs}$ .

Establishing this SARIMA model enables an accurate quantity of RL policies by capturing temporal patterns of the data. Achieving the effectiveness of the follow-up evaluation process of the predictive reward.

2) *Bayesian Prior Distribution of SARIMA Parameters*: In this section, the unknown parameters of the ARIMA model in the SARIMA model are estimated. By integrating the prior experience of traffic data properties, the SARIMA model achieves effective evaluation for the RL policies in the next step. Firstly, the determination of the prior distribution of unknown parameters  $\xi = (c, \phi_1, \dots, \phi_p, \theta_1, \dots, \theta_q, \sigma^2)$  is a pivotal step for this section. Specifically, due to the non-negativity of history rewards  $R_{his}^i$ , the Truncated Normal distribution  $TN(\mu_c, \sigma_c^2, a, b)$  is suitable for the intercept term  $c$ . Where  $\mu_c$  is the mean of the untruncated normal distribution,  $\sigma_c^2$  is the variance of the untruncated normal distribution,  $a$  and  $b$  are the lower and upper bounds of the truncation interval, respectively. And due to the complexity of the traffic environment, incorporating a sparsity-inducing prior is essential when modeling history rewards  $R_{his}^i$ . Consequently, the Laplace distribution  $Laplace(\mu_{\phi_i}, b_{\phi_i})$  and Laplace distribution  $Laplace(\mu_{\theta_j}, b_{\theta_j})$  are selected for autoregressive coefficients  $\phi_i$  and moving average coefficients  $\theta_j$ , respectively. Where  $\mu_{\phi_i}$  and  $\mu_{\theta_j}$  are the means,  $b_{\phi_i}$  and  $b_{\theta_j}$  are the scale parameters, with a smaller  $b$  indicating a stronger tendency toward coefficient sparsity. Furthermore, the random error term  $\epsilon_t$  in RL has large uncertainties, thereby the Inverse Gamma distribution  $IGa(a_{\sigma^2}, b_{\sigma^2})$  is applied to estimate the variance  $\sigma^2$  of the random error term  $\epsilon_t$ . Where  $a_{\sigma^2}$  is the shape parameter and  $b_{\sigma^2}$  is the scale parameter. The heavy-tailed nature of this distribution effectively captures the potential for larger variance values. Above all, the prior distribution can be expressed as follows:

$$p(c) = \frac{1}{\sigma_c} \cdot \frac{\phi\left(\frac{c - \mu_c}{\sigma_c}\right)}{\Phi\left(\frac{b - \mu_c}{\sigma_c}\right) - \Phi\left(\frac{a - \mu_c}{\sigma_c}\right)} \quad (11)$$

$$p(\phi_i) = \frac{1}{2b_{\phi_i}} \exp\left(-\frac{|\phi_i - \mu_{\phi_i}|}{b_{\phi_i}}\right) \quad (12)$$

$$p(\theta_j) = \frac{1}{2b_{\theta_j}} \exp\left(-\frac{|\theta_j - \mu_{\theta_j}|}{b_{\theta_j}}\right) \quad (13)$$

$$p(\sigma^2) = \frac{b_{\sigma^2}^{a_{\sigma^2}}}{\Gamma(a_{\sigma^2})} (\sigma^2)^{-a_{\sigma^2}-1} \exp\left(-\frac{b_{\sigma^2}}{\sigma^2}\right) \quad (14)$$

where  $\xi = (c, \phi_1, \dots, \phi_p, \theta_1, \dots, \theta_q, \sigma^2)$  are all the parameters to be estimated, and  $\Phi(x) = \frac{1}{\sqrt{2\pi}} e^{-\frac{x^2}{2}}$

After obtaining the prior distribution of each parameter, the sample set  $\{\xi^{(1)}, \xi^{(2)}, \dots, \xi^{(N_t)}\}$  can be generated by random

sample. And the values set  $\{\hat{r}_{t+h}^{(i)}\}$  using each sample  $\{\xi^{(i)}\}$  at future time  $t+h$  can be calculated by Eq. (10).

The above process achieves effective estimation of the SARIMA parameters. Despite the high levels of uncertainty and instability present in history rewards data  $R_{his}^i$ , this process enables the acquisition of reliable sampled RL reward values set  $\{\hat{r}_{t+h}^{(i)}\}$ . In complex traffic environments, the history rewards always fail to serve as robust statistical metrics. Thereby the reasonableness of the RL policies is struggled to evaluate by traditional methods. Conversely, by leveraging the prior experience, the influence of these limitations can be effectively addressed. The above process establishes a foundation for conducting a reasonable and comprehensive evaluation of RL policies in subsequent analyses. Thereby enhancing the reliability and effectiveness of RL policies for ATSC.

3) *Bayesian Credible Interval for RL Reward*: In this section, the Bayesian credible interval for RL reward values  $\hat{r}_{t+h}^{(i)}$  is constructed to evaluate the reasonableness of the RL policies. Based on the RL reward values set  $\{\hat{r}_{t+h}^{(1)}, \hat{r}_{t+h}^{(2)}, \dots, \hat{r}_{t+h}^{(Nt)}\}$ , the Bayesian credible interval is calculated by the percentiles of this sample set. Specifically, this paper constructs a 95% Bayesian credible interval; take the 2.5th and 97.5th percentiles of the posterior sample values set:

$$CI_{Bayes95\%} = \left( \{\hat{r}_{t+h}^{(i)}\}_{2.5\%}, \{\hat{r}_{t+h}^{(i)}\}_{97.5\%} \right) \quad (15)$$

This interval represents the range within which the future value  $r_{t+h}^{(i)}$  falls with a 95% probability, given the observed data and the prior information.

Building on the above interval, the predictive reward  $r_{t+h}^i$  that is generated by the prediction network can be evaluated through the Bayesian credible interval. If the predictive reward falls within the range of the Bayesian credible interval, the RL policies will be employed. Conversely, the policies need to be fine-tuned.

### C. The Tune Layer

The Bayesian decision-based Tune Layer is responsible for fine-tuning RL policies by posterior risk when the evaluation is negative. This layer ensures the RL policies adapt to real-time traffic conditions, enhancing the reasonableness of the policy-making process. The tuning process is divided into two main sections.

1) *The Incorporating of Q-values Information*: This section mainly involves determining the prior distribution of history Q-values  $Q_{his}^{i(j)}$  and constructing the Q-values  $\{Q_{cur}^{i(j)}, Q_{his}^{i(j)}\}$  likelihood function. Firstly, given the high entropy inherent in traffic environments, Q-values often exhibit multiple peaks and may present a noninformative prior. For this complexity, this paper employs the Kernel Density Estimation (KDE), a nonparametric Bayesian method, to estimate the probability density function of history Q-values. This estimated density is then utilized to construct the prior distribution:

$$\hat{f}(Q) = \frac{1}{Th} \sum_{t=1}^T K \left( \frac{Q - Q_t^{i(j)}}{bw} \right) \quad (16)$$

where  $bw$  is the bandwidth parameter,  $K(u)$  is the Gauss kernel, in which  $K(u) = \frac{1}{\sqrt{2\pi}} \exp(-\frac{u^2}{2})$

Concurrently, the likelihood function of Q-values can be constructed, which includes two parts. Specifically, based on the Gauss kernel, the likelihood function of the history Q-values  $Q_{his}^{i(j)}$  is defined as the follows:

$$\begin{aligned} L(Q_t^{i(j)}|Q) &= K \left( \frac{Q - Q_t^{i(j)}}{bw} \right) \\ &= \frac{1}{\sqrt{2\pi}bw^2} \exp \left( -\frac{(Q - Q_t^{i(j)})^2}{2bw^2} \right) \end{aligned} \quad (17)$$

Additionally, since the current Q-value  $Q_{cur}^{i(j)}$  carries greater significance in RL-based policy-making process, a confidence-based weighting mechanism is designed. This paper uses the normal distribution with an error term to describe the likelihood of the current Q-value, denoted as the "weighted likelihood function":

$$L(Q_{cur}^{i(j)}|Q) = \frac{1}{\sqrt{2\pi}\sigma_{cur}^2} \exp \left( -\frac{(Q - Q_{cur}^{i(j)})^2}{2\sigma_{cur}^2} \right) \quad (18)$$

where  $\sigma_{cur}^2$  is a tuning parameter representing the uncertainty of the current Q-value. A smaller  $\sigma_{cur}^2$  value means higher confidence in the current Q-value. This adjustment allows the Tune layer to prioritize the most recent state information, which is crucial for capturing the dynamic nature of traffic flow.

By combining the weighted likelihood of the current Q-value  $L(Q_{cur}^{i(j)}|Q)$  with the history Q-value prior distribution  $\hat{f}(Q)$ , the overall likelihood function is expressed as follows:

$$L(Q) = L(Q_{cur}^{i(j)}|Q) \times \prod_{t=1}^T L(Q_t^{i(j)}|Q) \quad (19)$$

This integrated likelihood function enhances the adaptability and responsiveness of the RL agent to real-time traffic conditions. Ensuring comprehensive and effective subsequent Bayesian-based phase tuning.

2) *Bayesian Posterior Risk of Each Phase*: In this section, the Bayesian posterior risk of each phase is calculated to refine the RL policies. As in the Critique Layer, the Bayesian posterior distribution is initially updated according to *Bayes' theorem*:

$$p(Q|Q_{cur}^{i(j)}, \{Q_t^{i(j)}\}) \propto L(Q) \times \hat{f}(Q) \quad (20)$$

Subsequently, based on the Bayesian decision theory, a loss function  $L(Q_{cur}^{i(j)}, Q)$  is introduced to measure the posterior risk (this paper adopts the square loss function  $L(Q_{cur}^{i(j)}, Q) = (Q_{cur}^{i(j)} - Q)^2$ ). The expected posterior risk for each phase in the intersection  $I_i$  is expressed as follows:

$$\mathcal{R}_{post} = \int_{\Theta} L(Q_{cur}^{i(j)}, Q) p(Q|Q_{cur}^{i(j)}, \{Q_t^{i(j)}\}) dQ \quad (21)$$

Building on the Bayesian criteria, the posterior risk for each phase is computed, and the phase that minimizes the expected posterior risk  $\mathcal{R}_{post}$  is selected as the optimal action:

$$\min \mathcal{R}_{post} = \inf_j \int_{\Theta} L(Q_{cur}^{i(j)}, Q) p(Q|Q_{cur}^{i(j)}, \{Q_t^{i(j)}\}) dQ \quad (22)$$

Under the square loss function  $L(Q_{cur}^{i(j)}, Q) = (Q_{cur}^{i(j)} - Q)^2$ , it can be theoretically proven that the above process minimizes the posterior risk (the detailed proof is presented in Appendix B). Thereby leading to the most effective policy refinement for RL. This methodology ensures the selected phase achieves the lowest total policy-making risk, enhancing the reasonableness of the RL policies for ATSC.

#### IV. RL WITH ATTENTION-BASED ADAPTIVE PRESSURE FOR ATSC

This section presents the attention-based adaptive pressure RL for ATSC. In Subsection IV-A, an Attention-Based Adaptive Pressure (AP) is introduced. Subsection IV-B details the AP-based DQN for ATSC, which serves as the policy-making backbone of the total framework. Finally, Subsection IV-C outlines the policy-making and training process for the proposed BCT-APRL.

##### A. Attention-Based Adaptive Pressure Extraction

In the complex urban environment, effective and efficient traffic states representation of each lane is crucial for optimizing signal control. To achieve effectively capture the real-time traffic states, this paper proposes an Attention-Based Adaptive Pressure.

In an intersection  $I_i$ , the AP mechanism identifies the source upstream lane associated with each vehicle and links it to the corresponding downstream lane. The downstream lanes  $\{X_y^{i'}\}$  and upstream lanes  $\{X_y^i\}$  are represented as four-layer matrices of dimensions  $3 \times 3$ , where the matrices are denoted as  $K$  and  $Q$ , respectively. Each of the three columns in these matrices represents: the number of waiting vehicles  $k_{wai}$  and  $q_{wai}$ , the number of running vehicles  $k_{run}$  and  $q_{run}$ , and the total number of vehicles  $k_{tot}$  and  $q_{tot}$ . The three rows correspond to the left-turn lane *lef*, straight-through lane *str*, and right-turn lane *rig*. Besides, the four layers of the matrix represent the directions: east *E*, west *W*, south *S*, and north *N*.

The AP mechanism further utilizes a multi-head attention mechanism to process and extract detailed information from both downstream and upstream lanes. This processed data are subsequently used as inputs for the query matrix  $Q$  and key matrix  $K$ . The multi-head attention mechanism is formalized as follows:

$$W_u^i = \psi_{\text{linear}}(\text{Concat}(W_1^i, W_2^i, \dots, W_{\text{head}}^i)) \quad (23)$$

where,

$$W_l^i = \text{Softmax} \left( \frac{q_l^i (K_l^i)^T}{\sqrt{d_k^i}} \right) \quad (24)$$

In this formulation, *head* represents the number of attention heads, and  $d_k$  is the dimensionality of the key  $K$ . This multi-head attention mechanism allows the AP system to construct a four-layer upstream attention weight matrix with dimensions  $3 \times 3$ . This matrix represents the weight of vehicle number influence of each upstream lane on three downstream lanes. A higher attention weight signifies a stronger impact. Based on these attention weights and Eq. (2), the AP can be obtained. Unlike traditional methods that treat the queue lengths of all

downstream lanes as coming equally from each upstream lane. AP achieves adaptability and effective capture of the traffic states, avoiding the lackness of traditional methods. Wherein these weaknesses may amplify the impact of low-traffic lanes while weakening responsiveness to high-traffic ones.

##### B. AP-based DQN for ATSC

In the ATSC, this paper adapts the RL method using Deep Q-Networks (DQN), tailored to optimize the traffic signal phase policy-making process at intersections. The AP-based DQN algorithm employs artificial neural networks (ANNs) to approximate the optimal action-value function  $Q(s_t^i, a_t^i)$  for each phase selection at each time step  $t$ . The architecture of AP-based DQN for ATSC is shown in Fig. 4. This dual-network framework comprises both an online network and a target network, with parameters  $\zeta$  and  $\zeta^*$  respectively. These two networks maintain the same structure but are updated at different rates to stabilize the learning process.

For AP-based DQN signal control in an intersection  $I_i$ , the state  $s_t^i$  is indicated as the current traffic conditions, which include the AP, the intersection phase, the number of running vehicles of upstream lanes, and the spatial correlation of each intersection. These state information forms the basis upon which the DQN estimates  $Q^{n_t^i}(s_t^i | \zeta)$ , enabling the system to select the optimal traffic signal phase  $j \in J_i$  for minimizing congestion and delay at the intersection. Besides, the action space  $A$  consists of predefined signal phases, and the objective is to maximize the cumulative reward by optimizing the traffic flow. The reward  $r_t^i$  is designed to reflect traffic efficiency, integrating both a phase-switching penalty and a traffic throughput incentive. A negative reward is imposed for unnecessary phase switching. In contrast, a positive reward is provided for improvements in transportation efficiency.

By interacting with experience replay pool  $\omega$ , DQN improves learning efficiency by storing all replay experience  $\{(s_t^i, a_t^i, r_t^i, s_{t+1}^i), \dots, (s_{st}^i, a_{st}^i, r_{st}^i, s_{st+1}^i)\}_{i=1}^n$  of one epoch  $st$ , and computing the following gradient by differentiating the loss function with respect to the weights:

$$\nabla_{\zeta} L(\zeta) = \alpha \eta_t \nabla_{\zeta} Q(s_t^*, a_t^*; \zeta) \quad (25)$$

where  $\alpha$  denotes the learning rate,  $s_t^*, a_t^*$  belongs to the target network, and the temporal-difference (TD) error  $\eta_t = \{r_t^*, \dots, \eta_t^{n^*}\}$  is calculated as:

$$\eta_t^{i^*} = r_t^{i^*} + \gamma \max_{a_{t+1}^{i^*}} Q(s_{t+1}^{i^*}, a_{t+1}^{i^*}; \zeta^*) - Q(s_t^{i^*}, a_t^{i^*}; \zeta) \quad (26)$$

The online network parameters  $\zeta$  are updated by stochastic gradient descent and Eq. (25). And the target network parameters  $\zeta^*$  are updated via soft updates:

$$\zeta^* \leftarrow \tau \zeta + (1 - \tau) \zeta^* \quad (27)$$

In this algorithm, the AP-based DQN framework effectively adapts to ATSC. Equipped with the AP, the system achieves a more refined and context-aware signal control. This adaptive algorithm minimizes average travel time at urban intersections, making the RL policies efficiently responsive to fluctuating traffic conditions.

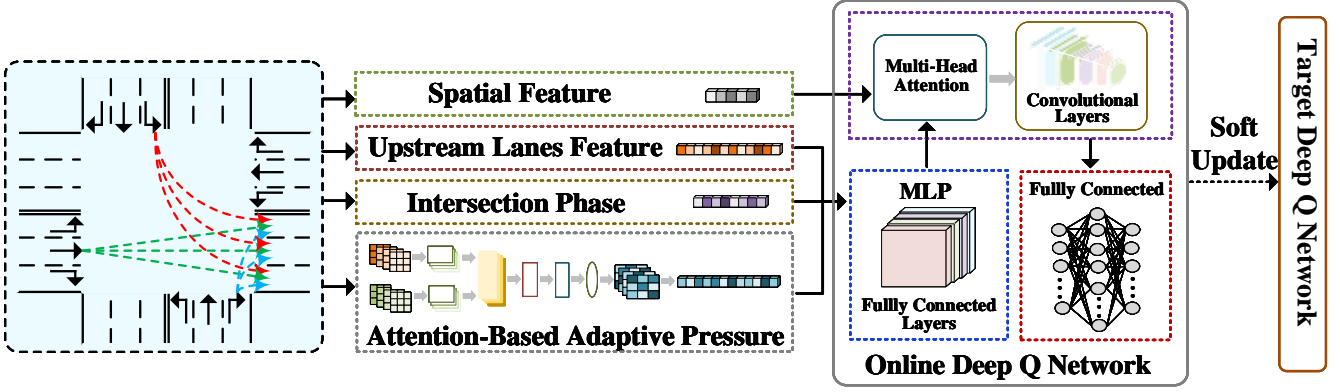


Fig. 4: Architecture of attention-based upstream pressure extraction for each intersection direction.

---

**Algorithm 1:** BCT-APRL Policy-Making and Training Algorithm for Multi-Intersections

---

**Input:** DQN-based agents for multi-intersections  $\{I_i\}_{i=1}^n$  ATSC;

**Output:** Optimized signal phase policies for all intersections  $\{\pi_{upd}^i\}_{i=1}^n$ ;

```

1 Initialize experience replay pool  $\omega$ ;
2 Initialize online network  $\zeta$ , target network  $\zeta^* \leftarrow \zeta$ , and
  auxiliary prediction network;
3 for  $t = 1$  to  $T$  do
4   for  $episode = 1$  to  $max\_epoch$  do
5     Initialize traffic states  $s_0^i$  for intersection  $I_i$ ;
6     Obtain history rewards  $R_{his}^i$  and history
       Q-values  $Q_{his}^{i(j)}$  from replay buffer  $\epsilon^i$ ;
7     for  $I_i$  in  $\{I_i\}_{i=1}^n$  do
8       Obtain current Q-values  $Q_{cur}^{i(j)}$  to select
          action  $a_t^i$  using  $\epsilon$ -greedy policy;
9       Obtain predictive reward  $r_{t+h}^i$  using the
          auxiliary prediction network;
10      Critique Layer: Use  $R_{his}^i$  to construct
          credible interval  $CI_{Bayes}$ ; Evaluate if
           $r_{t+h}^i \in CI_{Bayes}$ ;
11      if  $r_{t+h}^i \notin CI_{Bayes}$  then
12        Tune Layer: Use  $\{Q_{cur}^{i(j)}, Q_{his}^{i(j)}\}$  to
          compute posterior risk  $\mathcal{R}_{post}$  for each
          phase; Update policy  $\pi_{upd}^i$  by obtaining
          the phase with  $\min \mathcal{R}_{post}$ ;
13      end
14      Observe next state  $s_{t+1}^i$  and reward  $r_t^i$ ;
15      Store transition  $(s_t^i, a_t^i, r_t^i, s_{t+1}^i)$  in  $\omega$ ;
16      Update  $\zeta$  via gradient descent  $\nabla_{\zeta} L(\zeta)$ ;
17      if Done then
18        break;
19      end
20    end
21    Update  $\zeta^* \leftarrow \tau \zeta + (1 - \tau) \zeta^*$ ;
22  end
23 end
24 return Optimal RL policies  $\{\pi_{upd}^i\}_{i=1}^n$  of intersections;

```

---

*C. BCT-APRL Policy-Making and Training Process*

The policy-making and training process of the BCT-APRL for multi-intersections is illustrated in Algorithm 1. Firstly, a DQN-based agent for ATSC is employed for multiple intersections  $\{I_i\}_{i=1}^n$ . With the initialization of the experience replay pool  $\omega$ , the online network  $\zeta$ , target network  $\zeta^* \leftarrow \zeta$ , and auxiliary prediction network are initialized for all intersections  $\{I_i\}_{i=1}^n$ . For each intersection, the algorithm follows an episodic method to facilitate learning, updating the networks iteratively.

During each episode, the algorithm initializes the traffic states  $s_0^i$ , retrieves history rewards  $R_{his}^i$  and history Q-values  $Q_{his}^{i(j)}$  from the experience replay pool  $\omega$ . Subsequently, for each time step  $t$  within each episode, the current Q-values  $Q_{cur}^{i(j)}$  are obtained using the  $\epsilon$ -greedy policy to select the most suitable action  $a_t^i$ . Concurrently, the predictive reward  $r_{t+h}^i$  is predicted using the auxiliary prediction network, providing a forecast for next performance.

Within each time step, the Critique layer is employed to evaluate the credibility of the predicted reward. The history rewards  $R_{his}^i$  are used to construct a Bayesian credible interval  $CI_{Bayes}$ . If the predicted reward  $r_{t+h}^i$  falls outside this credible interval, the algorithm activates the Tune Layer. This layer updates the policy by calculating posterior risk  $\mathcal{R}_{post}$  using the current Q-values  $Q_{cur}^{i(j)}$  and the history Q-values  $Q_{his}^{i(j)}$ , selecting the signal phase with the lowest risk.

The agent then observes the next state  $s_{t+1}^i$  and corresponding reward  $r_t^i$ , which is subsequently used to update the online network via gradient descent. Besides, the agent stores the transition tuple  $(s_t^i, a_t^i, r_t^i, s_{t+1}^i)$  in each replay buffer, ensuring the necessary experience is recorded for future use. After processing all time steps, the target network  $\zeta^*$  is updated based on the online network, ensuring stability in the learning process.

At the end of the process, the global optimal signal phase RL policies  $\{\pi_{upd}^i\}_{i=1}^n$  for all intersections are returned, culminating the training phase.

V. EXPERIMENTS AND RESULTS

To empirically evaluate the BCT-APRL, extensive experiments are conducted. Subsection V-A describes the overall



experiment settings. Subsection V-B provides the analysis of experiment results in detail. The ablation study is shown in the V-C.

### A. Experiment Setup

1) *Environment Settings*: This paper conducts experiments on the CityFlow traffic simulator [41], which is open-sourced and simulates the kind of data that is collected at real-world intersections for ATSC. In the environment, each road has three lanes, which the number 0 corresponds to the left-turn lane, number 1 corresponds to the straight-through lane, and number 2 corresponds to the right-turn lane. Following most existing methods, the minimum action duration is set at 30 seconds, and a three-second yellow signal and a two-second all-red time follow each green signal to prepare the transition. Besides, this paper employs an epsilon decay strategy modeled as a power function, with a minimum epsilon value set at 0.2 during the training phase. Following the completion of training, epsilon decay is disabled (epsilon decay set to 0) for model evaluation in the testing phase.

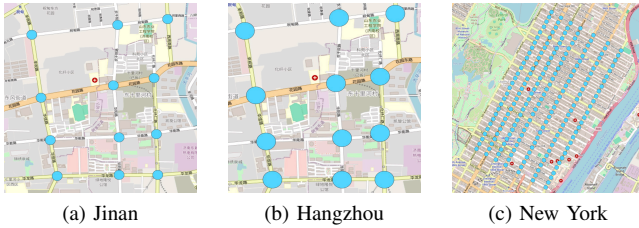


Fig. 5: The road network systems of the datasets from Jinan, Hangzhou, and New York, with uniform dimensions. The blue dots mark the traffic signal lights controlled by RL-agent.

2) *Datasets*: The experiments are conducted on seven real-world traffic flow datasets, including three datasets in Jinan( $3 \times 4$ ), two datasets in Hangzhou( $4 \times 4$ ), and two datasets in New York( $28 \times 7$ ). There are four directions (E,W,S,N) at each intersection. Each direction has an incoming road and an outgoing road, and each road has three lanes: left-turn lane, straight-through lane, right-turn lane. The visualization of three areas is shown in Fig. 5.

3) *Baselines*: For evaluating the effectiveness of BCT-APRL, this paper compares it with three transportation methods, six RL-based methods, and one LLM-based method.

Transportation methods:

- Random: A baseline method switches signal phases at random with a fixed duration.
- FixedTime [42]: Generally used in the majority of traffic situations, a method provides a pre-defined set cycle duration with phase time.
- MaxPressure [43]: The SOTA ATSC method in the traditional transportation field, maximizing traffic throughput by giving preference to the signal phase with the most traffic pressure.

RL-based methods:

- MPLight [44]: A RL-based method that utilizes pressure as both observation and reward, and extends FRAP method as its foundational model.

- AttendLight [45]: Introducing attention mechanism to state space and action space of RL.
- PressLight [46]: Optimizing the pressure of the intersection by utilizing the MaxPressure concept with DRL.
- CoLight [47]: Employing the graph attention network among intersections, to capture the neighborhood information and enhance the coordination ability of the RL agent.
- Efficient-CoLight [48]: Building upon the CoLight model. Introducing the concept of efficient pressure, which is noticing the equal length of entering lanes.
- Advanced-CoLight [39]: Building upon the CoLight model. Considering both the running and waiting vehicles to incorporate advanced traffic states features.

LLM-based method:

- LightGPT [49]: Introducing the Large Language Models into ATSC, leveraging the reasoning and decision-making process akin to human intuition for effective traffic control.

4) *Metrics*: Following previous studies [39], this paper leverages average travel time (ATT), average waiting time (AWT), and average queue length (AQL) of vehicles to evaluate the performance of each method.

- Average traveling time (ATT): The average traveling time measures the average duration of all the vehicles traveling from their starting points to their final destinations.
- Average queue length (AQL): The average queue length is defined as the average number of queuing vehicles waiting in the road network system.
- Average waiting time (AWT): The average waiting time measures the average queuing time of vehicles in line at each intersection in the road system

### B. Results and Analysis

1) *Overall Performance*: This paper evaluates the proposed methods using five real-world traffic flow datasets from Jinan and Hangzhou. Table I presents a comparative analysis of BCT-APRL and existing methods. The experimental results demonstrate that BCT-APRL consistently achieves state-of-the-art (SOTA) across all baselines. Among all existing methods, transportation methods generally underperform compared to RL-based methods and LightGPT. In transportation methods, MaxPressure exhibits relatively strong performance. Advanced-CoLight achieves the best results among all traditional RL-based methods. Although LightGPT is built upon the Large Language Model (LLM), it does not consistently outperform the traditional RL-based method, Advanced-CoLight. In comparison, BCT-APRL achieves competitive results by employing effective traffic states representation and evaluation mechanisms, further highlighting its exceptional effectiveness.

To comprehensively assess the overall and average performance of RL-based methods, this paper evaluates the train process of BCT-APRL alongside four high-performing traditional RL methods: Advanced-CoLight, Efficient-CoLight, CoLight, and PressLight. As shown in Fig. 6, all methods achieve satisfactory convergence, with BCT-APRL demonstrating superior

TABLE I: Overall performances of BCT-APRL and previous traditional methods on Jinan and Hangzhou datasets. The best results are highlighted through boldface

Method	Jinan									Hangzhou					
	Dataset-1			Dataset-2			Dataset-3			Dataset-1			Dataset-2		
	ATT	AQL	AWT	ATT	AQL	AWT	ATT	AQL	AWT	ATT	AQL	AWT	ATT	AQL	AWT
Random	604.32	693.25	101.46	565.03	434.52	103.42	622.04	292.18	95.16	632.41	325.86	75.19	601.35	689.71	94.55
FixedTime	464.35	471.23	78.05	412.03	275.33	65.04	432.23	385.31	68.03	513.04	187.92	63.64	420.65	396.73	68.97
MaxPressure	298.03	191.61	48.86	280.21	114.09	41.39	279.22	149.24	43.77	319.82	36.28	61.82	328.59	173.97	68.82
MPLight	303.19	210.45	95.23	301.02	137.04	87.67	289.65	167.92	86.58	353.28	87.21	85.23	362.67	241.60	103.51
AttendLight	292.35	184.33	63.21	282.84	116.92	54.28	271.03	142.87	54.68	320.54	65.29	60.92	355.23	230.47	70.61
PressLight	294.96	189.58	46.20	284.52	117.69	42.09	277.89	146.72	42.09	349.08	84.61	49.53	361.98	233.76	79.90
CoLight	280.26	167.41	57.05	271.52	105.89	53.85	264.17	130.08	48.99	315.24	67.73	60.87	332.02	189.16	86.43
Efficient-CoLight	276.48	176.27	47.41	269.93	102.94	39.51	264.27	130.43	42.37	308.49	55.33	32.15	337.03	185.85	67.63
Advanced-CoLight	274.27	157.36	48.40	266.82	100.29	43.51	262.38	128.32	43.04	300.90	48.46	39.27	326.61	168.53	73.55
LightGPT	277.60	166.17	48.21	272.24	104.93	48.78	261.34	129.27	45.02	316.40	61.55	49.92	333.42	190.43	68.99
<b>BCT-APRL</b>	<b>267.83</b>	<b>147.88</b>	<b>43.34</b>	<b>260.83</b>	<b>93.19</b>	<b>37.28</b>	<b>253.95</b>	<b>117.74</b>	<b>38.90</b>	<b>292.84</b>	<b>42.77</b>	<b>30.65</b>	<b>312.52</b>	<b>143.48</b>	<b>59.74</b>

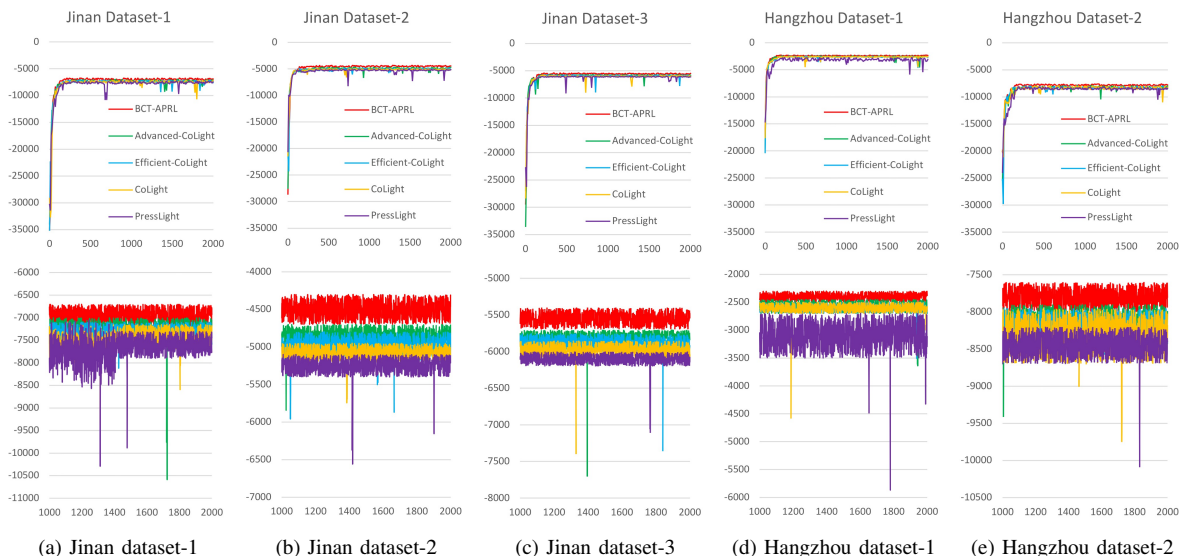


Fig. 6: The twin line chart of the rewards for each dataset in Jinan and Hangzhou. The upper section illustrates the overall trends of each method over 2000 episodes, while the lower section zooms into a smaller value range, highlighting subtle differences across 1000 episodes after convergence.

performance across the board, consistently outperforming the other methods.

2) *Stability Comparison*: To further compare the performance between BCT-APRL and other methods after convergence. Fig. 7 provides two three-group box plots to visualize the average data distribution of ATT, AQL, and AWT in the Jinan and Hangzhou datasets. In detail, the box plot is constructed based on the five-number summary of the data, which includes the minimum, first quartile (Q1), median, third quartile (Q3), and maximum values. The interquartile range (IQR) is calculated as  $IQR = Q3 - Q1$  to determine the lower and upper limits  $Q1 - 1.5 \times IQR$  and  $Q3 + 1.5 \times IQR$  to identify potential outliers, while the whiskers extend to the nearest data points within the range. Among the evaluated methods, BCT-APRL demonstrated superior performance consistently

across all metrics. This superiority is indicated by its smaller median values and a narrower range in the distribution. In particular, all existing methods exhibit some outliers, whereas BCT-APRL only presents seldom outliers, and the deviation is much smaller. This phenomenon indicates the ability of BCT-APRL to make effective and reasonable policies across all intersections.

3) *Large-Scale Intersections Experiment*: This paper conducts a comprehensive scalability analysis of traditional methods and BCT-APRL, evaluating their performance on a significantly larger road network, New York. Fig. 8 provides two two-group bar charts to visualize the data distribution of ATT and AWT in the New York datasets. The results indicate that BCT-APRL achieves the shortest travel and waiting times, underscoring its exceptional scalability and applicability to substantially larger road networks.

TABLE II: RESULTS OF ABLATION STUDY

Method	Jinan									Hangzhou					
	Dataset-1			Dataset-2			Dataset-3			Dataset-1			Dataset-2		
	ATT	AQL	AWT	ATT	AQL	AWT	ATT	AQL	AWT	ATT	AQL	AWT	ATT	AQL	AWT
DQN	368.43	270.35	100.06	345.71	205.93	106.42	327.11	249.68	96.06	427.65	143.26	93.99	440.62	307.35	143.61
AP-Based DQN	268.45	151.00	47.54	263.75	96.87	40.16	255.61	119.90	41.21	295.83	44.30	36.29	317.62	148.49	60.52
Advanced-CoLight	274.27	157.36	48.40	266.82	100.29	43.51	262.38	128.32	43.04	300.90	48.46	39.27	326.61	168.53	73.55
CT-Based Advanced-CoLight	270.53	152.67	45.65	264.16	97.58	40.04	257.09	121.10	42.05	297.00	45.34	33.26	317.06	157.13	69.41
BCT-APRL	<b>267.83</b>	<b>147.88</b>	<b>43.34</b>	<b>260.83</b>	<b>93.19</b>	<b>37.28</b>	<b>253.95</b>	<b>117.74</b>	<b>38.90</b>	<b>292.84</b>	<b>42.77</b>	<b>30.65</b>	<b>312.52</b>	<b>143.48</b>	<b>59.74</b>

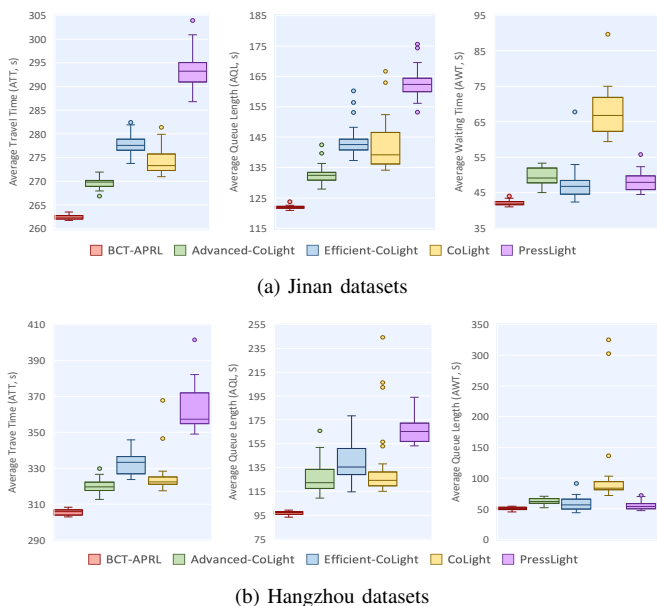


Fig. 7: The comparative results obtained using only the CT framework.

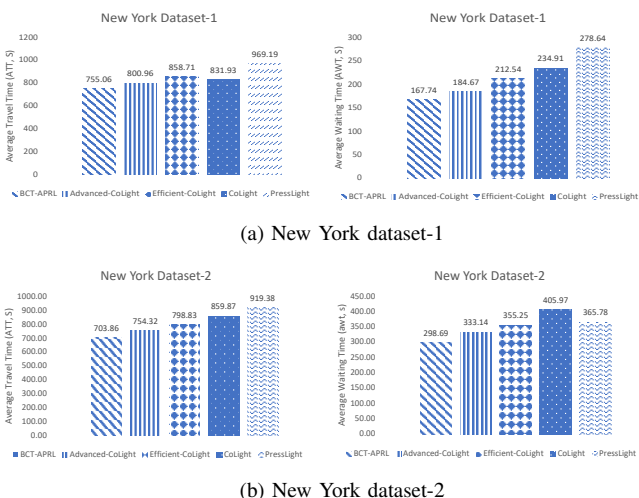


Fig. 8: The comparative results obtained using only the CT framework.

### C. Ablation Study

This section evaluates the performance of each component in BCT-APRL, namely the CT framework and the AP mechanism. In detail, this section firstly compares the performance

of the original DQN algorithm with the AP-based DQN. In addition, to explore the effectiveness of the CT framework, it is incorporated into the convergence model of Advanced-CoLight (the best method of traditional methods) to further train. As shown in Fig. II, the AP-based DQN significantly outperforms the original DQN algorithm. Moreover, the CT framework consistently surpasses Advanced-CoLight, demonstrating its ability to enhance the effectiveness of RL-based methods. Given that Advanced-CoLight demonstrates the best performance among all traditional methods, the results further reveal that even with only the AP mechanism applied, the performance still surpasses all of the methods. Notably, the removal of either component results in a marked degradation of the model's performance, emphasizing the critical role of both. Overall, this analysis underscores the indispensable role of each component in improving performance, reaffirming their collective value in advancing the capabilities of ATSC.

## VI. CONCLUSION

In this paper, a novel RL-based method (called BCT-APRL) is proposed for optimizing multi-intersection TSC. The BCT-APRL integrates two innovative components: the Critique-Tune (CT) framework and the Attention-Based Adaptive Pressure (AP). The CT framework leverages a two-layer Bayesian structure to refine reinforcement learning policies. Among it, the Critique layer employs Bayesian inference to evaluate the credibility of policies, while the Tune layer minimizes posterior risks to fine-tune policies when the evaluation is negative. This hierarchical mechanism ensures a robust policy refinement process, enabling more effective decision-making under varying traffic conditions. Meanwhile, the AP mechanism introduces an adaptive traffic movement representation that uses attention-based modeling to compute an effective and efficient pressure metric for vehicle queues, thereby enhancing the practicality and precision of the RL policies. Experiments conducted across seven real-world datasets with diverse intersection layouts validate the superiority of BCT-APRL over existing state-of-the-art methods. The results demonstrate that BCT-APRL achieves shorter travel times, reduced queue lengths, and improved traffic flow efficiency, highlighting its scalability and robustness in real-world traffic scenarios. In the future, the predictive accuracy of the prediction network can be further enhanced by incorporating more advanced modeling techniques or integrating additional real-time traffic data. Furthermore, the transferability of BCT-APRL across diverse traffic scenarios and network layouts is a promising avenue for exploration, ensuring its adaptability and scalability

to address future challenges in transportation efficiency and smart city development.

#### APPENDIX A

##### PROOF OF THE IDENTICAL ARIMA MODELS IN SARIMA

According to Eq. 8 and Eq. 7, applying the zero-mean transformation to the differenced series  $w_t^{i(d)}$ :

$$y_{n,i(d)} = w_t^{n,i(d)} - \bar{w}_t^{i(d)} \quad (28)$$

where  $\bar{w}_t^{i(d)}$  is the mean of the  $n - th$  episode differenced series.

Given that the mean does not affect stationarity:

$$\begin{aligned} E[y_t^{n,i(d)}] &= E[w_t^{n,i(d)} - \bar{w}_t^{i(d)}] \\ &= E[w_t^{n,i(d)} - \bar{w}_t^{i(d)}] - \bar{w}_t^{i(d)} \\ &= 0 \end{aligned} \quad (29)$$

the variance and autocorrelation structure thus remain unchanged:

$$\text{Var}(y_t^{n,i(d)}) = \text{Var}(w_t^{n,i(d)}) \quad (30)$$

$$\text{Cov}(y_t^{n,i(d)}, y_t^{n+s,i(d)}) = \text{Cov}(w_t^{n,i(d)}, w_t^{n+s,i(d)}) \quad (31)$$

Therefore,  $y_t^{n,i(d)}$  remains stationary.

Assume that the original differenced series  $w_t^{i(d)}$  follows the ARIMA model with parameters  $\phi_k$  and  $\theta_j$ . Substituting  $y_t^{n,i(d)} = w_t^{n,i(d)} - \bar{w}_t^{i(d)}$  into the ARIMA model:

$$y_t^{n,i(d)} + \bar{w}_t^{i(d)} = \sum_{k=1}^p \phi_k (y_t^{n-k,i(d)} + \bar{w}_t^{i(d)}) + \epsilon_{n,i} + \sum_{j=1}^q \theta_j \epsilon_{n-j,i} \quad (32)$$

Expanding above equation:

$$\begin{aligned} y_t^{n,i(d)} &= \sum_{k=1}^p \phi_k y_t^{n-k,i(d)} + \epsilon_{n,i} + \sum_{j=1}^q \theta_j \epsilon_{n-j,i} \\ &\quad + \sum_{k=1}^p \phi_k \bar{w}_t^{i(d)} - \bar{w}_t^{i(d)} \end{aligned} \quad (33)$$

The term  $\sum_{k=1}^p \phi_k \bar{w}_t^{i(d)} - \bar{w}_t^{i(d)}$  simplifies to 0 because the ARIMA coefficients  $\phi_k$  satisfy the normalization property  $\sum_{k=1}^p \phi_k = 1$ . Therefore, the equation reduces to:

$$y_t^{n,i(d)} = \sum_{k=1}^p \phi_k y_t^{n-k,i(d)} + \epsilon_{n,i} + \sum_{j=1}^q \theta_j \epsilon_{n-j,i} \quad (34)$$

Overall, the aforementioned process shows that the zero-mean-transformed series  $y_t^{n,i(d)}$  follows the identical ARIMA model with the same parameters  $\phi_k$  and  $\theta_j$ .

#### APPENDIX B

##### PROOF OF THE BAYESIAN POSTERIOR RISK PROCESS

In the Bayesian statistical decision problem, the definition of risk function is expressed as follows:

$$R(\delta, \theta) = E[L(\delta, \theta)] = \int_{\mathcal{X}} L(\delta, \theta) f(x, \theta) dx \quad (35)$$

where  $\delta$  is the decision rule, and the average loss  $R(\delta, \theta)$  is defined as the risk function of  $\delta$ .

According to Wald's statistical decision theory, the only criterion for evaluating the decision rules  $\delta$  is the associated risk function. If there exists a decision rule  $\delta^*$  such that for all  $\theta \in \Theta$  satisfy  $R(\delta^*, \theta) \leq R(\delta, \theta)$ , the  $\delta^*$  is called an admissible decision rule or a uniformly better decision rule. In practice, such a decision rule is often absent. As a result, the criteria are always relaxed; the common method is to impose optimality conditions based on the Bayes criterion.

Given a risk function  $R(\delta, \theta)$  and a prior distribution  $H(\theta)$  on  $\theta$ , with the prior denoted by  $\pi(\theta)$ , the Bayes risk is defined as:

$$\begin{aligned} R_H(\delta) &= E^\theta[R(\delta, \theta)] = \int_{\Theta} R(\delta, \theta) dH(\theta) \\ &= \int_{\Theta} \left( \int_{\mathcal{X}} L(\delta, \theta) f(x, \theta) dx \right) dH(\theta) \end{aligned} \quad (36)$$

The decision rule that minimizes the Bayes risk is termed the Bayes solution, denoted as  $R_H(\delta^*)$ .

After that, suppose  $\theta$  is fixed, and the random variable  $X$  follows the distribution  $f(x|\theta)$ . When new data is observed, the posterior distribution of  $\theta$  is updated to  $H(\theta|x)$ , using the prior  $H(\theta)$  and likelihood  $f(x|\theta)$ . The risk function is now evaluated with respect to the posterior distribution:

$$R(\delta|x) = E^{\theta|x}[L(\delta, \theta)] = \int_{\Theta} L(\delta, \theta) dH(\theta|x) \quad (37)$$

This is called the posterior risk of the decision rule  $\delta$ . If there exists a decision rule  $\delta^*$  such that:

$$R(\delta^*|x) = \min_{\delta} R(\delta|x) \quad (38)$$

then  $\delta^*$  is called the Bayes solution that minimizes the posterior risk.

From the Eq. (36), the following expression holds:

$$\begin{aligned} R_H(\delta) &= E^\theta[R(\delta, \theta)] = \int_{\Theta} R(\delta, \theta) dH(\theta) \\ &= \int_{\Theta} \left[ \int_{\mathcal{X}} L(\delta, \theta) F(x|\theta) \right] dH(\theta) \\ &= \int_{\mathcal{X}} \left[ \int_{\Theta} L(\delta, \theta) d(\theta|x) dx \right] dF_m(x) \\ &= \int_{\mathcal{X}} R(\delta|x) dF_m(x) = E^X[R(\delta|x)] \end{aligned} \quad (39)$$

where  $F_m(x)$  is the marginal distribution of  $X$ , and  $f_m(x)$  is its density.  $E^\theta$  represents the expectation taken with respect to the prior distribution of  $\theta$ . Therefore, the Bayes risk can be written as  $E^X[R(\delta|x)]$  indicating that the Bayes risk is simply the expectation of the posterior risk with respect to the marginal distribution of  $X$ .

It can be shown that the decision rule  $\delta^*$  that minimizes the posterior risk  $R(\delta^*|x)$  is the Bayes solution under the prior distribution  $H(\theta)$ . Besides, this Bayes solution  $R_H(\delta^*)$  also minimizes the Bayes risk  $R_H(\delta^*)$ , as shown by the following:

$$\begin{aligned} R(\delta|x) &= \int_{\Theta} L(\delta, \theta) H(d\theta|x) \\ &\geq \int_{\Theta} L(\delta_H, \theta) H(d\theta|x) = R(\delta_H|x) \end{aligned} \quad (40)$$

By taking the expectation of both sides with respect to the marginal distribution  $F_m(x)$ , the following inequality is obtained:

$$\begin{aligned} R_H(\delta) &= \int_{\mathcal{X}} R(\delta|x)dF_m(x) \\ &\geq \int_{\mathcal{X}} R(\delta_H|x)dF_m(x) = R_H(\delta_H) \end{aligned} \quad (41)$$

Thus,  $\delta_H$  minimizes the Bayes risk and is the Bayes solution, which achieves the minimal risk of the policy-making process of RL in ATSC.

## REFERENCES

- [1] E. A. Etukudoh, A. Adefemi, V. I. Ilojiana, A. A. Umoh, K. I. Ibekwe, and Z. Q. S. Nwokiediegwu, "A review of sustainable transportation solutions: Innovations, challenges, and future directions," *World Journal of Advanced Research and Reviews*, vol. 21, no. 1, pp. 1440–1452, 2024.
- [2] M. Zhang, Z. Li, H. Si, L. Cheng, X. Zhou, and B. Wang, "Urban travel time and residential location choice: The impacts of traffic congestion," *Sustainable Cities and Society*, vol. 99, p. 104975, 2023.
- [3] M. Harleman, L. Harris, M. D. Willis, B. Ritz, P. Hystad, and E. L. Hill, "Changes in traffic congestion and air pollution due to major roadway infrastructure improvements in texas," *Science of The Total Environment*, vol. 898, p. 165463, 2023.
- [4] A. Wided, B. Assia, and B. Fatima, "Traffic management system and traffic light control in smart city to reduce traffic congestion," *International Journal of Automation and Smart Technology*, vol. 13, no. 1, pp. 2464–2464, 2023.
- [5] V. Tong, S. Souihi, H. A. Tran, and A. Mellouk, "Troubleshooting solution for traffic congestion control," *Journal of Network and Computer Applications*, p. 103923, 2024.
- [6] W. Yue, C. Li, Y. Chen, P. Duan, and G. Mao, "What is the root cause of congestion in urban traffic networks: Road infrastructure or signal control?" *IEEE Transactions on Intelligent Transportation Systems*, vol. 23, no. 7, pp. 8662–8679, 2022.
- [7] A. Haydari and Y. Yilmaz, "Deep reinforcement learning for intelligent transportation systems: A survey," *IEEE Transactions on Intelligent Transportation Systems*, vol. 23, no. 1, pp. 11–32, 2022.
- [8] M. Noaen, A. Naik, L. Goodman, J. Crebo, T. Abrar, Z. S. H. Abad, A. L. Bazzan, and B. Far, "Reinforcement learning in urban network traffic signal control: A systematic literature review," *Expert Systems with Applications*, vol. 199, p. 116830, 2022.
- [9] Y. Han, M. Wang, and L. Leclercq, "Leveraging reinforcement learning for dynamic traffic control: A survey and challenges for field implementation," *Communications in Transportation Research*, vol. 3, p. 100104, 2023.
- [10] J. Gajcin and I. Dusparic, "Redefining counterfactual explanations for reinforcement learning: Overview, challenges and opportunities," *ACM Comput. Surv.*, vol. 56, no. 9, apr 2024. [Online]. Available: <https://doi.org/10.1145/3648472>
- [11] S. Munikoti, D. Agarwal, L. Das, M. Halappanavar, and B. Natarajan, "Challenges and opportunities in deep reinforcement learning with graph neural networks: A comprehensive review of algorithms and applications," *IEEE Transactions on Neural Networks and Learning Systems*, pp. 1–21, 2023.
- [12] Y. Lei, D. Ye, S. Shen, Y. Sui, T. Zhu, and W. Zhou, "New challenges in reinforcement learning: a survey of security and privacy," *Artificial Intelligence Review*, vol. 56, no. 7, pp. 7195–7236, 2023.
- [13] R. Zhu, L. Li, S. Wu, P. Lv, Y. Li, and M. Xu, "Multi-agent broad reinforcement learning for intelligent traffic light control," *Information Sciences*, vol. 619, pp. 509–525, 2023.
- [14] M. Nie, D. Chen, and D. Wang, "Reinforcement learning on graphs: A survey," *IEEE Transactions on Emerging Topics in Computational Intelligence*, vol. 7, no. 4, pp. 1065–1082, 2023.
- [15] Y. Lei, D. Ye, S. Shen, Y. Sui, T. Zhu, and W. Zhou, "New challenges in reinforcement learning: a survey of security and privacy," *Artificial Intelligence Review*, vol. 56, no. 7, pp. 7195–7236, 2023.
- [16] M. Kejrival, E. Kildebeck, R. Steininger, and A. Shrivastava, "Challenges, evaluation and opportunities for open-world learning," *Nature Machine Intelligence*, pp. 1–9, 2024.
- [17] Y. Song, Y. Wu, Y. Guo, R. Yan, P. N. Suganthan, Y. Zhang, W. Pedrycz, S. Das, R. Mallipeddi, O. S. Ajani *et al.*, "Reinforcement learning-assisted evolutionary algorithm: A survey and research opportunities," *Swarm and Evolutionary Computation*, vol. 86, p. 101517, 2024.
- [18] A. K. Shakya, G. Pillai, and S. Chakrabarty, "Reinforcement learning algorithms: A brief survey," *Expert Systems with Applications*, vol. 231, p. 120495, 2023.
- [19] S. Lin, J. Hu, W. Ma, C. Zheng, and R. Li, "Integrated real-time signal control and routing optimization: A two-stage rolling horizon framework with decentralized solution," *Transportation Research Part C: Emerging Technologies*, vol. 165, p. 104734, 2024.
- [20] B. Zhou, Q. Zhou, S. Hu, D. Ma, S. Jin, and D.-H. Lee, "Cooperative traffic signal control using a distributed agent-based deep reinforcement learning with incentive communication," *IEEE Transactions on Intelligent Transportation Systems*, 2024.
- [21] L. Zhang, Q. Wu, J. Shen, L. Lü, B. Du, and J. Wu, "Expression might be enough: representing pressure and demand for reinforcement learning based traffic signal control," in *International Conference on Machine Learning*. PMLR, 2022, pp. 26 645–26 654.
- [22] T. Wang, Z. Zhu, J. Zhang, J. Tian, and W. Zhang, "A large-scale traffic signal control algorithm based on multi-layer graph deep reinforcement learning," *Transportation Research Part C: Emerging Technologies*, vol. 162, p. 104582, 2024.
- [23] L. Da, M. Gao, H. Mei, and H. Wei, "Prompt to transfer: Sim-to-real transfer for traffic signal control with prompt learning," in *Proceedings of the AAAI Conference on Artificial Intelligence*, vol. 38, no. 1, 2024, pp. 82–90.
- [24] M. Tan, "Multi-agent reinforcement learning: Independent vs. cooperative agents," in *Proceedings of the tenth international conference on machine learning*, 1993, pp. 330–337.
- [25] H. Zhao, C. Dong, J. Cao, and Q. Chen, "A survey on deep reinforcement learning approaches for traffic signal control," *Engineering Applications of Artificial Intelligence*, vol. 133, p. 108100, 2024.
- [26] X. Wang, L. Ke, Z. Qiao, and X. Chai, "Large-scale traffic signal control using a novel multiagent reinforcement learning," *IEEE Transactions on Cybernetics*, vol. 51, no. 1, pp. 174–187, 2021.
- [27] G. Hinton, "Distilling the knowledge in a neural network," *arXiv preprint arXiv:1503.02531*, 2015.
- [28] D. Ye, T. Zhu, Z. Cheng, W. Zhou, and P. S. Yu, "Differential advising in multiagent reinforcement learning," *IEEE Transactions on Cybernetics*, vol. 52, no. 6, pp. 5508–5521, 2022.
- [29] C. Zhu, D. Ye, T. Zhu, and W. Zhou, "Location-based real-time updated advising method for traffic signal control," *IEEE Internet of Things Journal*, vol. 11, no. 8, pp. 14 551–14 562, 2024.
- [30] F. Mao, Z. Li, Y. Lin, and L. Li, "Mastering arterial traffic signal control with multi-agent attention-based soft actor-critic model," *IEEE Transactions on Intelligent Transportation Systems*, vol. 24, no. 3, pp. 3129–3144, 2023.
- [31] B. Liu, W. Han, E. Wang, S. Xiong, L. Wu, Q. Wang, J. Wang, and C. Qiao, "Multi-agent attention double actor-critic framework for intelligent traffic light control in urban scenarios with hybrid traffic," *IEEE Transactions on Mobile Computing*, vol. 23, no. 1, pp. 660–672, 2024.
- [32] X. B. Song, B. Zhou, and D. Ma, "Cooperative traffic signal control through a counterfactual multi-agent deep actor critic approach," *Transportation Research Part C: Emerging Technologies*, vol. 160, p. 104528, 2024.
- [33] M. Turchetta, A. Krause, and S. Trimpe, "Robust model-free reinforcement learning with multi-objective bayesian optimization," in *2020 IEEE International Conference on Robotics and Automation (ICRA)*, 2020, pp. 10 702–10 708.
- [34] N. Zhang, X. Yang, H. Guo, H. Dong, and W. Ma, "Approximate inference of traffic flow state at signalized intersections using a bayesian learning framework," *IEEE Transactions on Intelligent Transportation Systems*, vol. 24, no. 5, pp. 4765–4776, 2023.
- [35] H. Wei, C. Chen, G. Zheng, K. Wu, and Z. Li, "Presslight: Learning max pressure control to coordinate traffic signals in arterial network," *Proceedings of the 25th ACM SIGKDD International Conference on Knowledge Discovery & Data Mining*, p. 1290–1298, 2019.
- [36] T. Xu, S. Barman, and M. W. Levin, "Smoothing-mp: A novel max-pressure signal control considering signal coordination to smooth traffic in urban networks," *Transportation Research Part C: Emerging Technologies*, vol. 166, p. 104760, 2024.
- [37] D. Tsitsokas, A. Kouvelas, and N. Geroliminis, "Two-layer adaptive signal control framework for large-scale dynamically-congested networks: Combining efficient max pressure with perimeter control," *Transportation Research Part C: Emerging Technologies*, vol. 152, p. 104128, 2023.